Mechanisms for segregating T cell receptor and adhesion molecules during immunological synapse formation in Jurkat T cells

Yoshihisa Kaizuka*, Adam D. Douglass*, Rajat Varma†, Michael L. Dustin†‡, and Ronald D. Vale*‡

*The Howard Hughes Medical Institute and the Department of Cellular and Molecular Pharmacology, University of California, San Francisco, CA 94158; and †Program in Molecular Pathogenesis, Department of Pathology, Helan and Martin Kimmel Center for Biology and Medicine of the Skirball Institute, New York University School of Medicine, New York, NY 10016

Contributed by Ronald D. Vale, November 2, 2007 (sent for review October 2, 2007)

T cells interacting with antigen-presenting cells (APCs) form an ''immunological synapse'' (IS), a bull's-eye pattern composed of a central supramolecular activation cluster enriched with T cell receptors (TCRs) surrounded by a ring of adhesion molecules (a peripheral supramolecular activation cluster). The mechanism responsible for segregating TCR and adhesion molecules remains poorly understood. Here, we show that immortalized Jurkat T cells interacting with a planar lipid bilayer (mimicking an APC) will form an IS, thereby providing an accessible model system for studying the cell biological processes underlying IS formation. We found that an actin-dependent process caused TCR and adhesion proteins to cluster at the cell periphery, but these molecules appeared to segregate from one another at the earliest stages of microdomain formation. The TCR and adhesion microdomains attached to actin and were carried centripetally by retrograde flow. However, only the TCR microdomains penetrated into the actin-depleted cell center, whereas the adhesion microdomains appeared to be unstable without an underlying actin cytoskeleton. Our results reveal that TCR and adhesion molecules spatially partition from one another well before the formation of a mature IS and that differential actin interactions help to shape and maintain the final bull's-eye pattern of the IS.

actin | membrane microdomain | planar lipid bilayer | single-molecule imaging | supramolecular activation cluster

The activation of T cells during an immune response begins with contact and the formation of a stable junction between the T cell and an APC. Soon after their initial contact, substantial rearrangement of molecules occur on the plasma membranes of both cells. The TCR–peptide–major histocompatibility complex (MHC), cytoplasmic signaling proteins, and adhesion molecules [e.g., the integrin leukocyte function-associated antigen (LFA)-1 on the T cell and its ligand, intercellular adhesion molecule (ICAM)-1, on the APC] concentrate at the cell–cell interface and segregate into a distinctive structure known as the immunological synapse (IS) (1, 2). The IS consists of a central supramolecular activation cluster (cSMAC) that is highly enriched in the T cell receptor (TCR) and its associated peptide–MHC (pMHC) and is surrounded by a peripheral ring [peripheral (p)SMAC] of the LFA-1–ICAM-1 adhesion proteins (1, 2). Because of its high concentration of the TCR and other signaling molecules, it was originally thought the IS might be needed for sustained signaling, which is required for T cell activation (2). However, recent theories have proposed that the IS might be a site of TCR inactivation and endocytosis (3–9).

The mechanism for forming the micrometer-sized "bull's eye" pattern of the IS has been the subject of extensive investigation. An important breakthrough was achieved with the demonstration that an IS will form when a primary T cell interacts with a planar lipid bilayer containing pMHC and ICAM-1, thus removing the requirement for the APC in studying this reaction (2). An initial and influential hypothesis proposed that proteins segregated into the cSMAC and pSMAC based on the different sizes of their extracellular domains (10, 11). However, more recently, it has been shown that pMHC induces the formation of numerous submicrometer-sized TCR clusters that are centripetally transported by treadmilling actin filaments and then accumulate in the center (7–9, 12–14). Thus, actin-based transport of TCR to the center appears to explain the formation of the cSMAC. TCR microdomains continue to form at the periphery and are transported to the center long after initial cell contact, suggesting that the TCR may recycle from the cSMAC to the cell periphery (9, 15). The continual production of TCR-enriched membrane microdomains (which are enriched in other signaling proteins) appears to be important for sustaining T cell signaling (7–9, 16, 17). In contrast to the TCR and the cSMAC, very little is known about how adhesion molecules organize into pSMAC and how and/or when TCR and adhesion molecules separate from one another.

Although TCR, adhesion proteins, and actin have been shown to be critical molecules in IS formation, to our knowledge, no study to date has examined the dynamics of all three components in the same cell system. To facilitate such an imaging study, we sought to observe IS formation by using an immortalized Jurkat T cell line. The Jurkat T lymphoma line has certain advantage over primary cells for studying basic cell biological processes such as IS formation, because they are easily transfected and can be used in forward- and reverse-genetics experiments to probe signaling and cytoskeletal mechanisms (18). Although the pMHC activator of the TCR on Jurkat cells is unknown, anti-TCR antibodies activate early signaling events such as actin-induced cell spreading (17) through the WAVE complex and HS-1 (19, 20) and calcium release from the endoplasmic reticulum (18). In addition, it has been shown that signaling molecules and membrane receptors become organized in microdomains at the interface between Jurkat cells and an anti-TCR-coated glass surface (16, 17). However, because the adsorbed anti-TCR antibodies are immobile, the clusters of signaling molecule remain stationary and do not reorganize into an IS.

Here, we show that Jurkat cells form an IS when interacting with a glass-supported planar lipid bilayer containing TCR stimulatory molecules (monoclonal antibodies to the CD3ε subunit) and adhesion molecules (ICAM-1). By using Jurkat

Author contributions: Y.K. and A.D.D. contributed equally to this work; Y.K., A.D.D., and R.D.V. designed research; Y.K. and A.D.D. performed research; R.V. and M.L.D. contributed new reagents/analytic tools; Y.K. and A.D.D. analyzed data; and Y.K., A.D.D., and R.D.V. wrote the paper.

The authors declare no conflict of interest.

‡To whom correspondence may be addressed. E-mail: dustin@saturn.med.nyu.edu or vale@cmp.ucsf.edu.

This article contains supporting information online at www.pnas.org/cgi/content/full/0710258105/DC1.

cells transfected with GFP–actin, we achieved, to our knowledge, the first high-resolution imaging of actin, TCR, and adhesion proteins during the early events of IS formation. We show that TCR and adhesion molecules are organized into separate microdomains early in their genesis at the cell periphery, revealing that these proteins segregate well in advance of IS formation. Coimaging with actin–GFP speckles revealed that the dynamic actin network centripetally transports TCR and adhesion microdomains and that differential actin interactions may be involved in partitioning adhesion and TCR proteins into pSMAC and cSMAC zones respectively. We also show that a diffusion barrier at the mature cSMAC may help to exclude adhesion molecules from this region. This work reveals several factors that help to segregate TCR from adhesion molecules, both at the level of small microdomains and at the larger-scale organization of the IS.

Results

Jurkat T Cells Form Immunological Synapses When Stimulated on Planar Lipid Bilayers. We sought to reconstitute IS formation by stimulating Jurkat T cells with planar lipid bilayers containing mobile adhesion molecules and the stimulatory anti-TCR antibodies (Fig. 1*A*), which we modeled after the methods of Carrasco *et al.* (21) for analysis of the B cell IS. Small unilamellar vesicles containing the ICAM-1 (labeled with Alexa-488 or unlabeled) and 0.02% biotinylated phosphatidylethanolamine with a caproyl spacer (biotin–CAP–PE) were deposited onto an acid-washed glass coverslip, creating a planar lipid bilayer. The biotin–CAP–PE was conjugated with fluorescently tagged streptavidin, and then monobiotinylated anti-TCR (CD3ε) antibodies were subsequently reacted with these lipid–biotin–streptavidin complexes to create a substrate with the minimal components required for IS formation. Both the anti-TCR antibodies and ICAM-1 diffused freely within the bilayer, and >90% of the molecules were mobile (data not shown).

When Jurkat cells adhered to the planar lipid bilayer, they extended large, lamella structures within 30 s of contact and spread to a diameter of 20–30 μm. This actin-based spreading required TCR signaling, because it did not occur on bilayers containing ICAM-1 alone (data not shown). In the subsequent 10–20 min, the majority (≈80%) of cells formed a bull's eye pattern consisting of a large, central cluster of stimulatory antibodies surrounded by a zone of ICAM-1 enrichment (Fig. 1*B*). This pattern, although somewhat variable between cells, closely resembled the IS organization observed previously with primary T cells interacting with pMHC-containing bilayers (2) or with APCs (1). Once formed, these patterns showed little change in morphology for over 1 h, except for a slight overall contraction in the contact area. The pattern of the LFA-1 (the T cell integrin) superimposed with the location of ICAM-1 in the pSMAC, as expected (Fig. 1*C*). Immunostaining also revealed phosphotyrosine accumulation, particularly in the pSMAC and the actin-rich distal region (data not shown), indicating that the anti-TCR antibody on the planar bilayer was inducing signaling in the Jurkat cells. Thus, contact with an ICAM-1/anti-TCR bilayer induces the formation of an IS in Jurkat cells, providing an opportunity for studying the molecular basis of pattern formation with high temporal and spatial resolution with a readily transfected cell line.

We next characterized the locations of the TCR-enriched cSMAC and adhesion molecule enriched pSMAC relative to the actin-rich lamella by using cells expressing actin–GFP. The cSMAC generally was present in the actin-depleted center of the cell. In contrast, the pSMAC formed at the interior boundary of the actin-rich lamella but did not extend much beyond. This is particularly evident when cortical actin–GFP and LFA-1 were imaged by total internal reflection fluorescence (TIRF) microscopy [Fig. 1*D* and supporting information (SI) Movie 1]. As

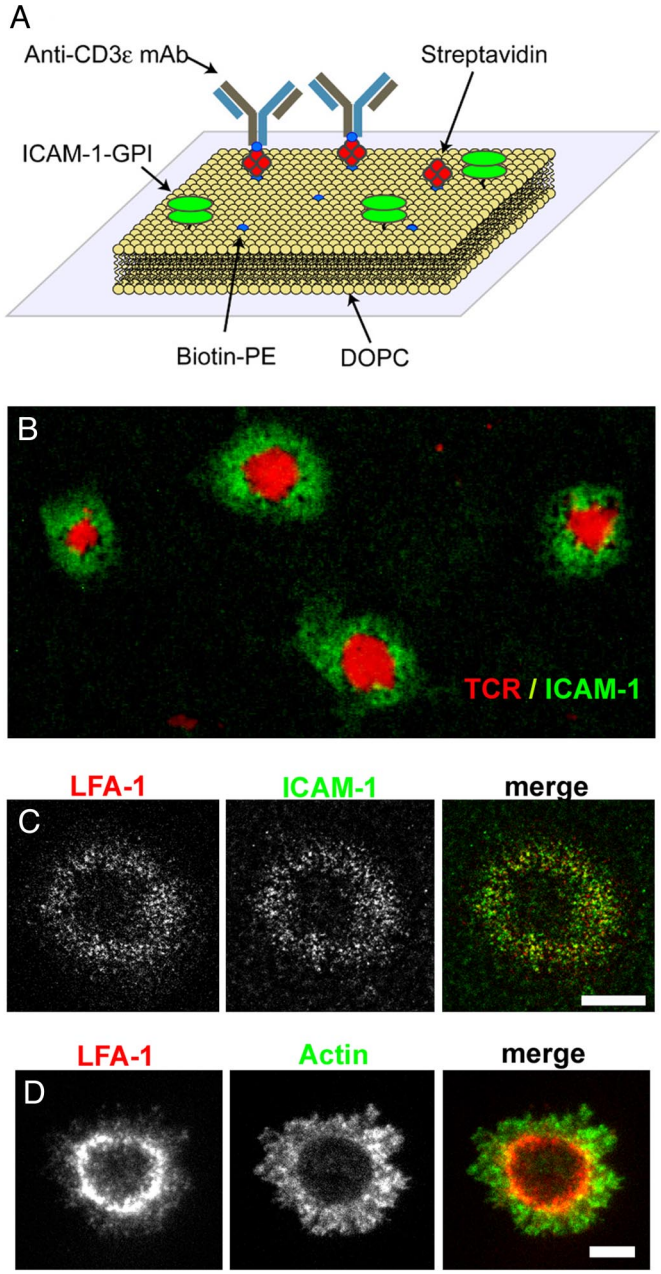

Fig. 1. Formation of an immunological synapse in Jurkat T cells interacting with planar lipid bilayers. (*A*) Schematic of the experimental system. Jurkat cells were adhered to planar lipid bilayers containing ICAM-1 (Alexa 488-conjugated) and anti-TCR antibodies (monobiotinylated anti-CD3ε antibodies bound to Texas red-conjugated streptavidin, which was attached to a biotinylated phospholipid) (see *Materials and Methods*). DOPC, dioleoylphosphocholine. (*B*) Confocal image of Jurkat cells bound to the lipid bilayer showing mature synapses at ≈30 min after initiation. Red indicates anti-TCR; green indicates ICAM-1. (*C*) Confocal image showing that ICAM-1 (green) and LFA-1 [labeled with cy3-conjugated anti-LFA-1 Fab (red)] colocalize at the pSMAC. (*D*) TIRF image of an actin–GFP expressing Jurkat cell at ≈30 min after initiation, showing that the pSMAC [labeled with cy3-anti LFA-1 Fab (red)] does not extend to the actin-poor cell center. (Scale bars, 5 μm.) Note that TIRF illumination tends to significantly amplify the intensity of surface proximal fluorophores in pSMAC and thus the pSMAC in *D* appears brighter than that in *C*.

described in other studies (9), the cSMAC was stable even after complete actin depolymerization with 40 μM latrunculin B (Lat B) (SI Fig. 6). In contrast to the cSMAC, the pSMAC zone was

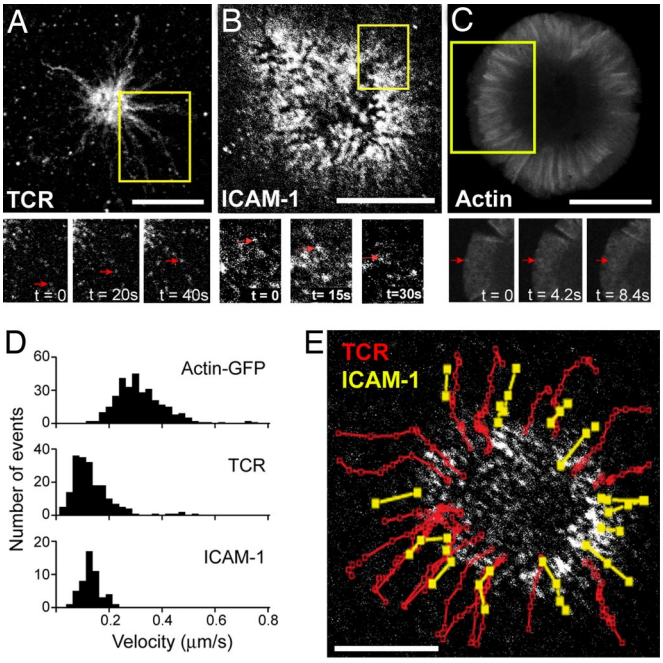

Fig. 2. Coupling of TCR and ICAM-1 microdomains to retrograde actin flow. Cells were applied to planar bilayers and imaged during the initial 10 min of synapse formation by spinning disk confocal microscopy. (*A*) (*Upper*) Maximum intensity projection of the TCR signal over a period of 4 min. Images were acquired at 1-s intervals. The majority of the bright fluorescent puncta are immobile aggregates of streptavidin in the bilayer. (Scale bar, 10 μm.) (*Lower*) Time course showing active transport of a single TCR microdomains (red arrow) in the ROI shown in the intensity projection. (*B*) (*Upper*) Maximum intensity projection of ICAM-1 over a period of 1 min. Images were acquired at 5-s intervals. (Scale bar, 10 μm.) (*Lower*) Time course showing retrograde movement of a single ICAM-1 microdomains over time. (*C*) (*Upper*) Maximum intensity projection of actin–GFP speckles over time. Images were acquired at 1.4-s intervals. (Scale bar, 10 μm.) (*Lower*) Time course showing retrograde movement of a single actin–GFP speckle (red arrow) in the boxed region shown in the intensity projection. (*D*) Histograms of transport rates of TCR (*Top*), actin–GFP (*Middle*), and ICAM-1 (*Bottom*) microdomains. (*E*) Trajectories of individual TCR (red) and ICAM-1 (yellow) microdomains, superimposed on an image of ICAM-1 in the mature synapse, reveal that TCR tends to have longer runs to the cell center. See SI Fig. 7 for more examples.

rapidly destabilized and dispersed after Lat B treatment (SI Fig. 6), as described previously (9).

Dynamics of IS Formation and Centripetal Actin-Driven Transport. We next examined the dynamics of IS formation. By using spinning disk confocal imaging, we observed the rapid coalescence of anti-TCR antibodies into microdomains at the actin-rich periphery of the bilayer-adhered Jurkat cell and their subsequent movement toward the center, following roughly linear paths (Fig. 2 *A* and *E* and SI Movie 2), similar to prior observations made with primary T cells on planar lipid bilayers (7–9). This movement was most dramatic within the first 10 min of cell–bilayer contact while the cSMAC was forming. However, even after 1 h, the formation of new TCR microdomains was still observed at the cell periphery. In agreement with prior studies (9), if actin nucleation/polymerization were inhibited by Lat B, *de novo* TCR microdomain formation was completely blocked (data not shown). However, once formed, TCR clustered in peripheral microdomains and in the cSMAC remained stable for at least 15 min after Lat B-mediated actin disassembly.

Fluorescently labeled ICAM-1 in the bilayers also concentrated into microdomains underneath the attached Jurkat cells, and these microdomains were transported centripetally toward the forming pSMAC (Fig. 2*B*). To our knowledge, this is the first time that adhesion protein microdomains have been described in T cells. Like the TCR, the formation and subsequent transport of ICAM-1 microdomains were both abolished by Lat B treatment (data not shown). Again, similar to the TCR, the formation of a new ICAM-1 microdomain could still be observed well after IS formation (≈1 h), suggesting a dynamic process and a mechanism for recycling.

To better understand the centripetal movement of TCR and ICAM-1 microdomains, we quantitatively examined the speed of microdomain translocation and compared them with that of actin filaments, which have not been directly examined in primary T cells. To observe actin filament movement, we imaged Jurkat cells expressing low levels of actin–GFP in which heterogeneities in fluorescence (speckles) could be observed and tracked (22). In the lamella of bilayer-adhered Jurkat cells, actin speckles moved radially inward from the distal edge of the lamella toward the center of the contact (SI Movie 2), analogous to the retrograde flow of actin seen in motile (22) and spreading cells (23). Kymograph analysis revealed that actin–GFP speckles moved at an average speed of 0.32 ± 0.01 μm/s (mean ± SEM; $n = 7$ cells in five bilayer samples; Fig. 2 *C* and *D*), which is one of the faster rates of retrograde actin flow observed in any system. The rate of TCR microcluster translocation was 2-fold slower than actin, with a mean velocity of 0.14 ± 0.006 μm/s (mean ± SEM: $n = 10$ cells in eight bilayer samples; Fig. 2 *A* and *D*). In GFP–actin-expressing Jurkat cells, it was clear that many of the TCR clusters formed at the very leading edge of the cell where actin is polymerizing (SI Movie 2). The rate of ICAM-1 centripetal movement was 0.13 ± 0.005 μm/s (mean ± SEM: $n =$ 3 cells in three bilayer samples; Fig. 2 *B* and *D*), which was comparable with TCR. From these measurements, we propose that the TCR and ICAM-1 move centripetally by linking to the underlying cytoskeleton; their slower rates of transport reflect slippage in the coupling mechanism to actin (duty ratio of ≈0.4). Note that translocation rate of each microdomain varied along its trajectory, and we measured the rates at the cell periphery where both TCR and ICAM-1 microdomains moved fastest.

Early Segregation of TCR and Adhesion Microdomains. Simultaneous imaging of ICAM-1 and TCR in the same cells revealed additional information about microdomain formation and patterning (Fig. 3 and SI Movie 3). Before IS formation (within 10 min), ICAM-1 and TCR formed ligand–receptor interactions in the periphery, but these signaling and adhesion molecules clustered into distinct microdomains that did not spatially overlap with one another (Fig. 3). Thus, ICAM-1 and TCR segregate from one another at the earliest stage of clustering at the cell periphery as well as at later stages of IS formation.

Imaging of ICAM-1 and TCR in the same cells also revealed that the lengths of trackable runs of ICAM-1 microdomains tended to shorter than those of the TCR (Fig. 2*E* and SI Fig. 7). The TCR could be followed for longer distances from the periphery to the site of the forming cSMAC; generally the bright TCR-enriched cSMAC precluded further tacking of microdomains near the center, rather than resulting from disappearance of the microdomain itself. Transported ICAM-1 microdomains, on the other hand, accumulated in the pSMAC region but rarely moved further into the actin-poor central region of the cell (Fig. 2*E* and SI Fig. 7).

The cSMAC Creates a Diffusion Barrier That Excludes Molecules. We next turned our attention to single-molecule imaging to gain further insight into the mechanism of IS formation. By using low concentrations of fluorescently labeled ICAM-1 molecules, single ICAM-1 molecules could be imaged diffusing in the bilayer. By tracking these molecules by semiautomated procedures (16), we noted that ICAM-1 molecules rarely penetrated into the

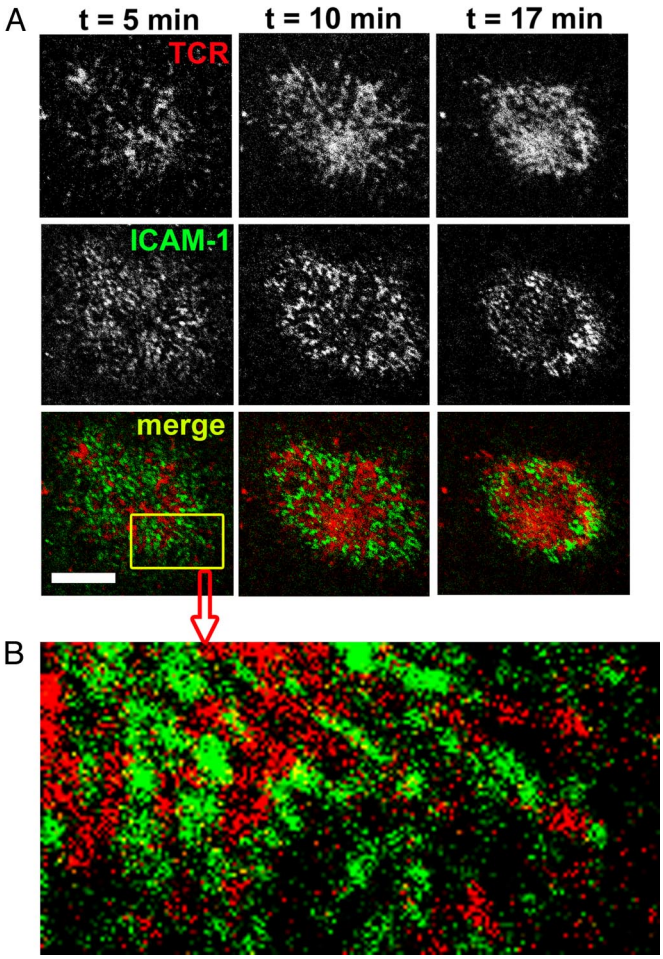

Fig. 3. Segregation of TCR and ICAM-1 microdomains occurs before IS formation. Cells were applied to stimulatory bilayers and imaged by spinning-disk confocal microscopy during the early stages of synapse formation. (*A*) Time-lapse images of TCR (anti-CD3, red) and ICAM-1 (green) show that microcluster formation and centripetal movements precede the formation of both the cSMAC and pSMAC. (*B*) A close-up view of the boxed region shown in *A* demonstrates segregation of TCR and ICAM-1 into spatially segregated microclusters at the periphery. (Scale bar, 5 μm.)

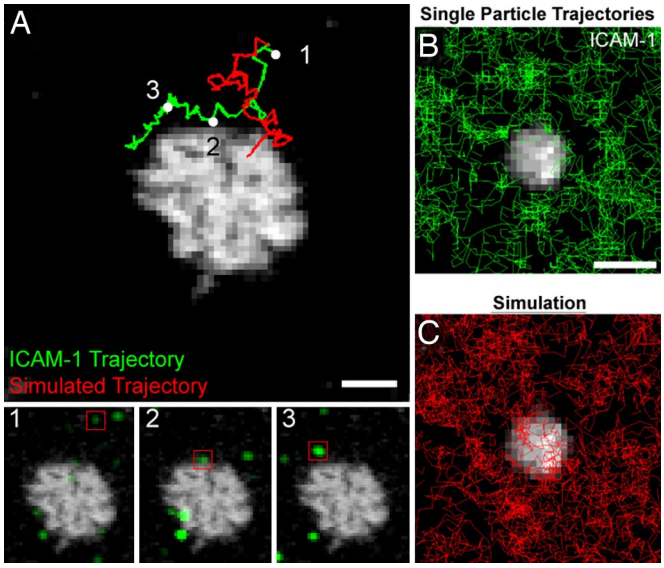

Fig. 4. The cSMAC creates a barrier to diffusion. A time series of single ICAM-1 molecules (imaged by TIRF) was superimposed on a single image of the cSMAC (fluorescent streptavidin linked to anti-TCR antibodies and imaged by epifluorescence), so that the behavior of single molecules could be analyzed relative to the boundaries of the cSMAC. (*A*) Trajectories of a single ICAM-1 particle (green) and its simulated counterpart (red) relative to a cSMAC, illustrating the simulation method. (Scale bar, 2 μm.) White dots indicate points illustrated in the bottom images, which show the single-molecule ICAM-1 images (green channel; red brackets) at three time points. The concentration of ICAM-1 molecules is comparable to other experiments, and the number of fluorescent ICAM-1 is adjusted for single-molecule imaging by photobleaching of most fluorophores. (*B* and *C*) Comparison of a population of real particles (*B*) and their simulated counterparts (*C*) in representative synapses (n = 252 trajectories). Particle trajectories were overlaid onto a population-level image of the cSMAC (grayscale). (Scale bar, 4 μm.)

center of the cSMAC and rather deflected off the edge of the cSMAC (Fig. 4*A* and SI Movie 4). This result suggests that the cSMAC may prevent the penetration of ICAM-1 molecules. To substantiate this conclusion, we compared an observed single molecule trajectory to the trajectory of a simulated random walk (beginning at the starting position as the single molecule and ending after the same amount of elapsed time) (Fig. 4). The simulated and real trajectories were then plotted with respect to the location of the cSMAC. As shown in Fig. 4*B* (typical of five cells analyzed in this manner), the ≈2- to 3-times more simulated trajectories crossed into the area of the cSMAC and these trajectories covered ≈10 times more area (including the area near very center of the cSMAC) than the actual measured trajectories did. This finding supports our conclusion that the cSMAC acts as a barrier to the free diffusion of ICAM-1 molecules.

Discussion

Several previous studies using primary T cells interacting with planar lipid bilayers have described the formation of TCR microdomains at the periphery and their retrograde transport toward the cell center (7–9). We replicated these findings (as well as IS formation) by using Jurkat T cells, indicating that this easily transfectable cell line constitutes a good model system for studying this phenomenon and can be used to complement work performed with native T cells. By using this system, we have performed the first high-resolution time-lapse imaging of adhesion molecules and actin during IS formation, thus providing an understanding of the dynamic properties of these proteins in relation to the TCR. Our results show that adhesion proteins segregate from the TCR at the cell periphery, revealing mechanisms that partitions these proteins well before IS formation. The TCR and adhesion microdomains attach to the retrogradely moving actin cytoskeleton, but their slower rates of centripetal transport compared with actin suggest that they are attached to actin for <50% of the time. Our results also suggest that adhesion molecules are linked to the inner zone of the actin cytoskeleton and do not populate the center because of the relative paucity of actin in that region and because of an exclusion effect of the protein-dense cSMAC zone. These observations suggest a sequence of events in IS formation (Fig. 5), which are described in more detail below.

Formation and Early Segregation of TCR and Adhesion Protein Microdomains. Our previous studies show the formation of protein microdomains when Jurkat T cells are stimulated by TCR antibodies fixed onto glass surfaces, but these microdomains are stationary because of the immobilization of the stimulating ligand on the glass (16). When the stimulatory molecules are adhered to a planar lipid bilayer, we now found remarkable dynamic behavior in which microdomains form continually at the periphery and move centripetally, as shown in previous work

CELL BIOLOGY

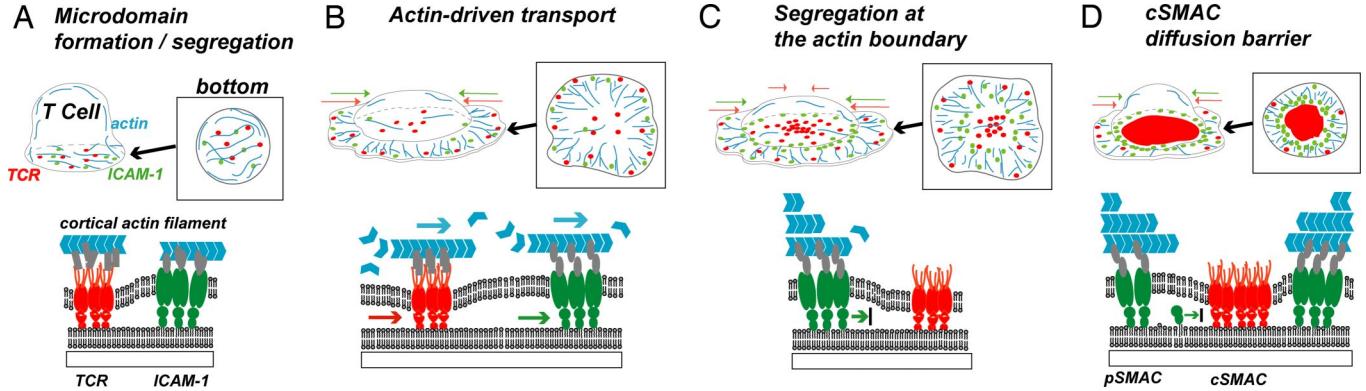

Fig. 5. The model for the segregation of TCR and adhesion molecules during the immunological synapse formation. Differential cluster nucleation, translocation, and diffusional exclusion of ICAM-1 and TCR drive immunological synapse formation. (*A*) At the initial contact of the Jurkat T cell with the planar lipid bilayer, interactions with the actin cytoskeleton form spatially separated TCR (red) and ICAM-1 (green) microdomains (note, ICAM–LFA-1 interactions likely form subsequent to TCR signaling). (*B*) After cells spread, separate TCR and ICAM-1 microdomains form primarily at the cell periphery, where new actin filaments are polymerizing. These microdomains are anchored to actin filaments and transported toward the cell center along with actin retrograde flow. (*C*) TCR microdomains populate the actin-sparse cell center and form the cSMAC, whereas ICAM-1 microdomains require anchoring to actin filaments for stability and do not extend beyond the actin boundary. (*D*) A diffusional barrier at the cSMAC periphery may hinder ICAM-1 from entering the mature cSMAC, thus helping to make the boundary.

(7–9). In addition to TCR microdomains, to our knowledge, this work provides the clearest evidence to date that the adhesion molecules (the integrin LFA-1 and its partner ICAM-1) also form microdomains. The TCR and adhesion microdomains are segregated from one another in the periphery, well in advance of SMAC formation. Even after the IS is formed, these microdomains continue to arise at the cell periphery as described for the TCR (7–9). Because the total areas of pSMAC and cSMAC do not change drastically for ≈1 h, LFA-1 and the TCR must be recycled from the pSMAC and cSMAC, respectively, to create new microdomains at the periphery.

Our imaging of TCR antibodies and ICAM-1 in the planar bilayer shows that new microdomains frequently form at the leading edge of the cell, where new actin is polymerizing. This observation indicates a very rapid reorganization of these molecules in the bilayer just after they encounter the surface receptors on the T cells and the underlying cytoskeleton (Fig. 5*A*). Presumably the actin filaments are facilitating or catalyzing the protein–protein interactions that underlie the formation of these microdomains. However, details on this mechanism are unclear at the present time.

Role of Actin in the Centripetal Motion and Stability of Microdomains. After microdomain formation, TCR and ICAM-1/LFA-1 clusters are carried centripetally by actin retrograde flow (Fig. 5*B*). Centripetal motion of the TCR has been shown previously in primary T cells (2, 9, 14), but, to our knowledge, this is the first demonstration for LFA-1 microdomains. By simultaneously imaging the TCR, ICAM-1, and actin for the first time, we were able to gain insight into pSMAC formation. We show that actin centripetal movement is more than twice as fast as that of the TCR and LFA-1. This difference in speed likely reflects a slippage among the TCR, LFA-1, and the associated proteins that mediate their attachment to the moving actin filament network (24).

Whereas TCR and adhesion microdomains both travel centripetally through connections to actin, the TCR microdomains tend to have a longer travel distance than adhesion microdomains and these TCR microdomains meet and coalesce in the cell center, producing the cSMAC (Fig. 5*C*). This distinct behavior may involve differences in how the TCR and adhesion molecules interact with the actin cytoskeleton. Once formed, the TCR microdomains are stable in the absence of actin, as shown by experiments with latrunculin (this work and ref. 9). Thus, TCR microdomains can populate the very cell center, which is relatively sparse in cortical actin compared with the periphery (Fig. 1*D*). These microdomains coalesce and form the cSMAC, as described by others (6–9). In contrast, the LFA-1 microdomains require actin for their stability (destabilized by latrunculin) and may not be stable in the actin-depleted cSMAC. Indeed, the disappearance of ICAM-1 microdomains at or near pSMAC-cSMAC boundary can frequently be observed (data not shown). We also observe the disappearance of ICAM-1–LFA-1 from the central contact shortly after the T cell contacts the planar lipid bilayer (Fig. 3*A*). One explanation for this disappearance could be attributable to the rearrangement of actin from an initially uniform cortical distribution to a peripheral, leading edge distribution as the cell spreads on the planar lipid bilayer. In contrast, TCR that is initially at the center of the contact remains there, even after the actin filament network redistribute during cell spreading.

A Diffusion Barrier at the cSMAC. After the cSMAC forms, our data suggest that this zone creates a diffusion barrier that further maintains the separation of the pSMAC and cSMAC (Fig. 5*D*). Previously, we have observed that small membrane microdomains that form during T cell signaling on glass surfaces coated with anti-TCR antibodies create barriers to entry of diffusing plasma membrane proteins (16). Based on the observed restricted entry of freely diffusing ICAM-1 in the supported membrane bilayer, we suggest that a similar phenomenon occurs for the cSMAC on a larger scale. At the present time, we favor the idea that the diffusion barrier is created by a very dense packing of proteins resulting from protein–protein interactions (16). However, we still know relatively little about the packing of proteins and the degree of permeability of the cSMAC. Future studies could probe this question in a more quantitative manner by using smaller (e.g., fluorescent lipids) and various sized protein molecules.

Molecular Basis of Microdomain Formation and Linkages to Actin. Whereas the phenomenon of microdomain formation is clear from this study, the molecules that mediate these processes remain to be elucidated. Because actin filaments are crucial for microdomain formation and centripetal transport, the TCR and integrins must be connected to actin filaments by specific linker

proteins. Previous studies have shown that LFA-1 colocalizes with talin-1 in pSMAC, as is also observed in focal adhesions (1). Thus, talin is a strong candidate to play a role in linking LFA-1 microdomains to actin, although a myriad other proteins may participate as well (25). The TCR may use a different set of actin linkers, and the actin-regulating adaptor molecules Nck or WASp have been implicated in such processes (26). However, other molecules might be responsible for connecting TCR microdomains to treadmilling actin and await discovery. Another remarkable observation from this work is the rapid separation of TCR and LFA-1–ICAM-1 into largely nonoverlapping microdomains. Although different lipid environments (e.g., lipid rafts) might contribute to such condensation processes, we envisage that the formation of these microdomains is driven primarily by protein–protein interactions. The physical separation of TCR and LFA-1 into separate patches on the membrane therefore may reflect distinct sets of protein scaffolds that build up on these liganded receptors. Although many interactions have been defined for the TCR and integrins by classic biochemical techniques, the list is undoubtedly incomplete. New methods will be required for defining the complete inventory of the proteins and protein–protein interactions that occur in TCR and LFA-1 microdomains.

Materials and Methods

Cells and Reagents. Jurkat T cells were maintained and transfected as described previously (16). All lipids were purchased from Avanti. Other reagents used in experiments are anti CD3ε monoclonal antibody Hit3a (BD), fluorescent streptavidin (Invitrogen), and Lat B (Sigma-Aldrich). Cy3-labeled anti-LFA-1 Fab (TS2/4) was prepared in similar way described previously (9) and used for labeling cells at 0.05–0.5 mg/ml on ice for 15 min before imaging.

Preparation of Planar Lipid Bilayers. Human ICAM-1–GPI was purified, fluorescently labeled, and incorporated into liposomes as previously described (27). Anti-CD3ε antibody was monobiotinylated following the procedure of Carrasco *et al.* (21). Liposomes that contained biotin–CAP–PE and dioleoylphosphocholine were mixed with ICAM-1 liposome at a 0.02 mole percentage final concentration of biotin–CAP–PE. Mixed liposomes were deposited on glass surface cleaned by piranha solution (a mixture of sulfuric acid and hydrogen peroxide) and a single fluid planar bilayer was created on the substrate under imaging buffer (HEPES buffer saline). Fluorescent streptavidin and monobiotinylated anti-CD3ε antibody were reacted sequentially and conjugated with biotinylated lipids in a planar bilayer.

Microscopy and Image Analysis. High-speed confocal images were acquired on a TE2000U inverted microscope (Nikon) or a 200M microscope (Zeiss) equipped with a Yokogawa spinning-disk confocal scan head (Solamere Technology Group), and images were captured with a Cascade II camera (Photometrics) or an Orca II ER CCD camera (Hamamatsu Photonics) by using μManager software (N. Amodaj, N. Stuurman, and R.D.V., University of California at San Francisco) or MetaMorph software (Molecular Devices). TIRF imaging with a TE2000U microscope (Nikon) equipped with a Cascade II camera (Photometrics) and scanning confocal imaging with an LSM510 microscope (Zeiss) was also performed. Single-molecule images were captured with a Mega 10 S30Z intensified camera (Stanford Photonics) installed on an Axiovert 200M (Zeiss) equipped with custom-built laser TIRF illumination optics and a $\times$100, 1.45 NA oil immersion objective (Zeiss). Single-molecule tracking was performed as described previously (16). By using a custom MATLAB script, we generated randomly oriented trajectories that simulated the mobility of ICAM-1 (Fig. 4*B*).

ACKNOWLEDGMENTS. We thank A. Weiss, J. Weissman, and M. Krummel for helpful discussions and T. Starr for technical help. A portion of the data for this study was acquired at the Nikon Imaging Center (University of California, San Francisco). This work was supported in part by a National Science Foundation predoctoral fellowship (to A.D.D.), a Bernard Levine fellowship (to R.V.), the National Institutes of Health (M.L.D.), and the Sandler Foundation (R.D.V.).

1. Monks CRF, Freiberg BA, Kupfer H, Sciaky N, Kupfer A (1998) *Nature* 395:82–86.
2. Grakoui A, Bromley SK, Sumen C, Davis MM, Shaw AS, Allen PM, Dustin ML (1999) *Science* 285:221–227.
3. Lee KH, Holdorf AD, Dustin ML, Chan AC, Allen PM, Shaw AS (2002) *Science* 295:1539–1542.
4. Freiberg BA, Kupfer H, Maslanik W, Delli J, Kappler J, Zaller DM, Kupfer A (2002) *Nat Immunol* 3:911–917.
5. Lee KH, Dinner AR, Tu C, Campi G, Raychaudhuri S, Varma R, Sims TN, Burack WR, Wu H, Wang J, *et al.* (2003) *Science* 302:1218–1222.
6. Mossman KD, Campi G, Groves JT, Dustin ML (2005) *Science* 310:1191–1193.
7. Yokosuka T, Sakata-Sogawa K, Kobayashi W, Hiroshima M, Hashimoto-Tane A, Tokunaga M, Dustin ML, Saito T (2005) *Nat Immunol* 6:1253–1262.
8. Campi G, Varma R, Dustin ML (2005) *J Exp Med* 202:1031–1036.
9. Varma R, Campi G, Yokosuka T, Saito T, Dustin ML (2006) *Immunity* 25:117–127.
10. Wild MK, Cambiaggi A, Brown MH, Davies EA, Ohno H, Saito T, van der Merwe PA (1999) *J Exp Med* 190:31–41.
11. Qi SY, Groves JT, Chakraborty AK (2001) *Proc Natl Acad Sci USA* 98:6548–6553.
12. Valitutti S, Dessing M, Aktories K, Gallati H, Lanzavecchia A (1995) *J Exp Med* 181:577–584.
13. Wulfing C, Davis MM (1998) *Science* 282:2266–2269.
14. Krummel MF, Sjaastad MD, Wulfing C, Davis MM (2000) *Science* 289:1349–1352.
15. Das V, Nal B, Dujeancourt A, Thoulouze MI, Galli T, Roux P, Dautry-Varsat A, Alcover A (2004) *Immunity* 20:577–588.
16. Douglass AD, Vale RD (2005) *Cell* 121:937–950.
17. Bunnell SC, Hong DI, Kardon JR, Yamazaki T, McGlade CJ, Barr VA, Samelson LE (2002) *J Cell Biol* 158:1263–1275.
18. Abraham RT, Weiss A (2004) *Nat Rev Immunol* 4:301–308.
19. Gomez TS, McCarney SD, Carrizosa E, Labno CM, Comiskey EO, Nolz JC, Zhu P, Freedman BD, Clark MR, Rawlings DJ, *et al.* (2006) *Immunity* 24:741–752.
20. Nolz JC, Gomez TS, Zhu P, Li S, Medeiros RB, Shimizu Y, Burkhardt JK, Freedman BD, Billadeau DD (2006) *Curr Biol* 16:24–34.
21. Carrasco YR, Fleire SJ, Cameron T, Dustin ML, Batista FD (2004) *Immunity* 20:589–599.
22. Ponti A, Machacek M, Gupton SL, Waterman-Storer CM, Danuser G (2004) *Science* 305:1782–1786.
23. Rogers SL, Wiedemann U, Stuurman N, Vale RD (2003) *J Cell Biol* 162:1079–1088.
24. Hu K, Ji L, Applegate KT, Danuser G, Waterman-Storer CM (2007) *Science* 315:111–115.
25. Mor A, Dustin ML, Philips MR (2007) *Immunol Rev* 218:114–125.
26. Barda-Saad M, Braiman A, Titerence R, Bunnell SC, Barr VA, Samelson LE (2005) *Nat Immunol* 6:80–89.
27. Dustin ML, Olszowy MW, Holdorf AD, Li J, Bromley S, Desai N, Widder P, Rosenberger F, van der Merwe PA, Allen PM, *et al.* (1998) *Cell* 94:667–677.